

## CHAPTER 6

### Experiments

The main aim of the experimental study described in this chapter is to investigate realization aspects and demonstrate practical viability of the proposed methods. The experimental case-study involves a electro-mechaniced motion system where the lowest frequency natural mode for the structure clearly dominates motion behaviour and tuning can be realized through a variable geometry design. The design of the experimental system was kept simple since it serves as a demonstration unit only.

#### 6.1 Experimental motion system

##### 6.1.1 Components

The test system was set up to perform linear translation of a flexible armature using a ball-screw drive with DC motor, as shown in Fig. 6.1. The main components are

- a Linear guide and ball screw bearing (Misumi SSEBWZ14.-470)
- b Variable stiffness flexible armature with end mass (original design)
- c Horizontal ball screw (Misumi BSSR1004-500-SC7)
- d D.C. motor with incremental encoder (Maxon motor 60 watt 24 volt RE30: 268214 with encoder 1024 count per turn(CPT) 3 channels: 225787)
- e Laser sensor to measure absolute position of end mass (Baumer electric CH-8501 Frauenfeld OADM 20I6472/S14F)
- f Strain gauge sensor to measure deflection of armature

The motor was driven by a Copley controls DC brush servo amplifier (models:4122Z) in current(torque)-control mode.

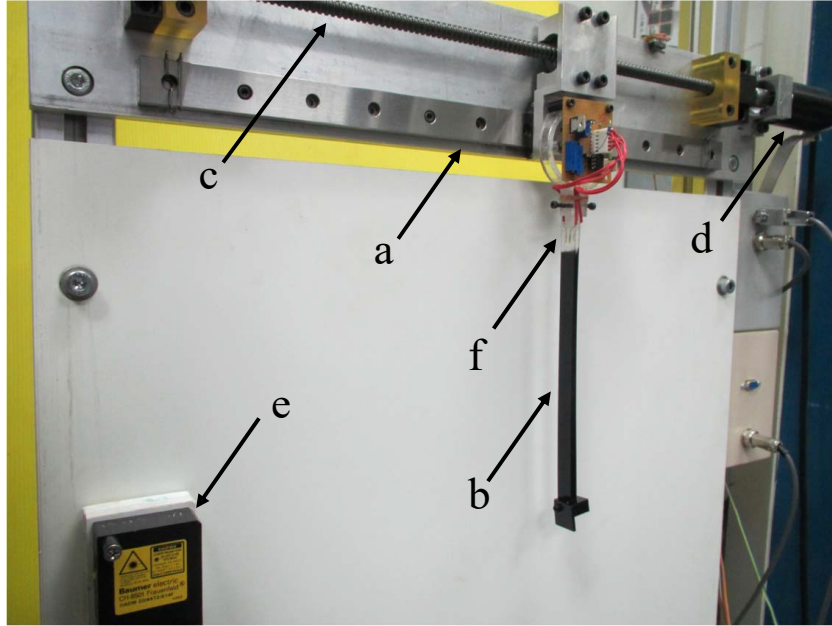


Figure 6.1: Experimental rig

To model the dynamics of the current-controlled d.c. motor, the following governing equation for the motor torque is adopted:

$$T_M(t) = K_T i(t), \quad (6.1)$$

where  $T_M(t)$  is the produced torque,  $K_T$  is motor torque constant and  $i(t)$  is the applied current. This equation is used under the assumption that any dynamic response (finite bandwidth) associated with the electrical drive can be neglected. The equation for rotating motion of the motor and ball screw is

$$I\ddot{\theta}(t) = T_M(t) - c_M\dot{\theta}(t) + T_f, \quad (6.2)$$

where  $\theta(t)$  is the angular position of the motor and  $I$  is the effective mass moment of inertia. Friction arising from the ball screw and other moving parts is represented by  $c_M$  for viscous friction and  $T_f$  for Coulomb friction. These effects are significant and must be accounted for in the model of the system. Therefore, the final form of the state-space equation of the rigid-body mode is

$$\begin{bmatrix} \dot{\theta}(t) \\ \ddot{\theta}(t) \end{bmatrix} = \begin{bmatrix} 0 & 1 \\ 0 & -\frac{c_M}{I} \end{bmatrix} \begin{bmatrix} \theta(t) \\ \dot{\theta}(t) \end{bmatrix} + \begin{bmatrix} 0 \\ \frac{K_T}{I} \end{bmatrix} i(t) + \begin{bmatrix} 0 \\ \frac{T_f}{I} \end{bmatrix} \quad (6.3)$$

This model represents the rigid-body dynamics only.

Parameters were identified by experimental tests involving acceleration measurements for various speeds and motor currents. Values for friction-related parameters  $c_M$  and  $T_f$  were determined by finding a compensating control current law (which relates to force via the motor constant  $K_T$ ) that was seen to best cancel the effects of friction. Use of a high bandwidth current-controlled servo drive means that the motor current may be considered as the system input, saturating at imposed limits of  $\pm 1$  Amp. Table 6.1 summarizes the notation and nominal parameter value for the experimental set-up and motor.

Table 6.1: Parameters of the experimental rig

Parameter	Notation	Value
Motor constant	$K_T$	25.9 mN.M/A
Current used for compensate viscous friction	-	0.6 amp
Current used for compensate coulomb friction	-	0.165 amp
Viscous friction coefficient	$c_M$	0.0362
Coulomb friction	$T_f$	0.099
Total inertia	$I$	$1.9 \times 10^{-5}$ kg.m <sup>2</sup>
ball screw's pitch for unit conversion	-	4 mm
Correlation coefficient of the variable stiffness device	$a_1$	0.0737
Resolution of incremental encoder	-	0.004 mm

### 6.1.2 Variable stiffness mechanism

The flexible armature consists of two uniform beams separated by a small gap which is fixed at one end while at the other end, the gap can be varied. By varying the gap via adjustment of the screws, the boundary condition of the flexible armature is changed and this alters the second moment of area of the beam cross-section. This produces a change in the overall stiffness, and thus natural frequency, of the structure. The armature has a payload/endmass of approximately 20 g. The diagram of the flexible armature with variable stiffness device is shown in Fig. 6.2.

The achievable range for tuning the value of the damped natural frequency was approximately 30 – 50 rad/s. To quantify how the imaginary part of the system pole varied with the real part, tap tests were undertaken and values calculated from the rate of exponential decay in vibration amplitude. These results are shown in Fig. 6.3. A linear approximation gives the value for the correlation coefficient  $a_1 = 0.0737$ , as appearing in (5.19).

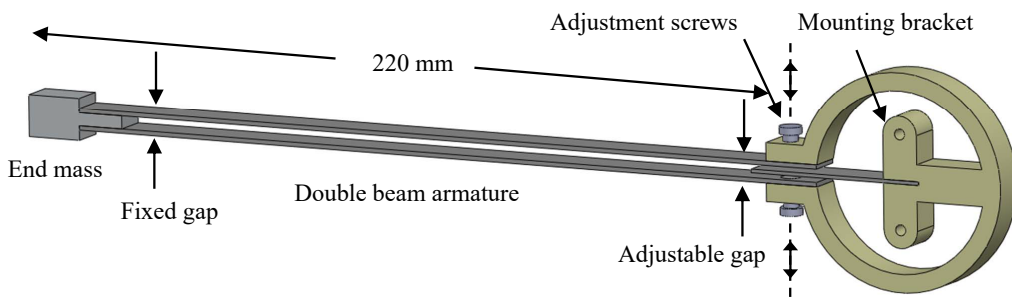


Figure 6.2: Variable stiffness flexible beam

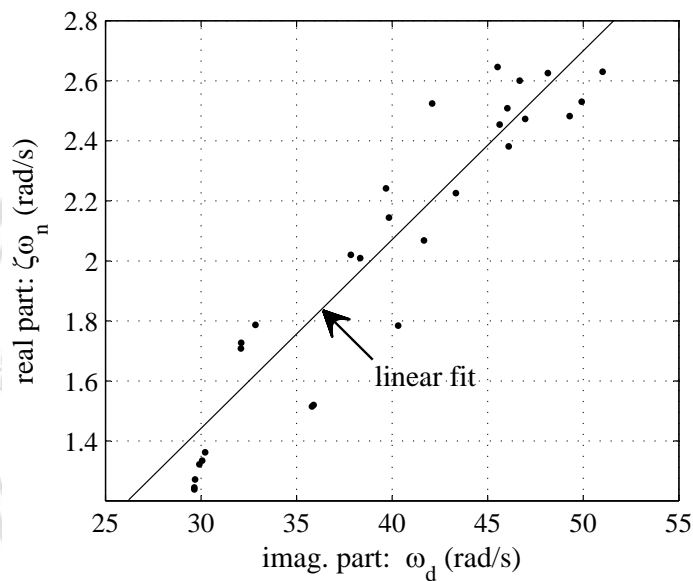


Figure 6.3: Experimental results showing correlation between real and imaginary parts of system poles under structural tuning

## 6.2 Feedback implementation

The time-optimal control input acquired using the methods in the chapter 3 is in open loop form and can feed directly into the system to achieve the projected zero vibration outcome. The experimental outputs are expected to be exactly the same as the calculated simulation results if the mathematical model of the test rig is perfectly determined. However, it is almost impossible to perfectly specify every parameter value for the test system. Moreover, the value of each parameter sometimes slightly change with each time the test is conducted. This might be because of some small particle in the ball screw causes non-smooth rotation and translation of the moving part or small differences in friction coefficients or other unknown issues may occur.

These small errors in the mathematical model tend to cause some residual vibration in the experiments. Due to the extreme effort to drive a system in the nature of the bang-bang solutions, the non-zero residual vibration might be surprisingly large compared with the expected zero residual vibration as obtained in the simulation. This behaviour corresponds with many claims in numerous research studies about time-optimal control that the time optimal control solutions have poor robustness to errors in system parameters. To deal with this problem, it may be assumed the main cause of the error is the friction and inertia of the system since these parameters cannot be measured directly unlike natural frequency and damping ratio. The feedback loop is therefore introduced into the control system to ensure that the actual position of the moving bearing part matches with the projected optimal trajectory which is simultaneously calculated in real-time.

Suppose  $G$  represents the actual dynamics of the system while  $\tilde{G}$  is the adopted model. A model reference feedback control structure can be adopted as shown in Fig. 6.4. A high gain controller  $K$  can be used to ensure the errors in the measure output are kept as small as possible. In this study a simple PD controller was used. The gains for this controller were chosen by using pole placement technique. The location of the poles are chosen to give quick response of the controller without changing the characteristics of the original system too much. The transfer function of the PD controller is:

$$\frac{30s + 1200}{0.0025s + 1} \quad (6.4)$$

With the proposed PD controller, the poles of the feedback loop are placed at  $10 \pm 30j$ . The block diagram of the overall control system is shown in Fig. 6.4. An additional control input from the feedback controller will disturb the bang-bang form of the solution. However, the error is small and thus the deviation from optimal condition is negligible.

### 6.3 Results

For the selected case study, the structural optimization problem started from a nominal set-up for which the damped natural frequency of the armature was 30 rad/s. A rest-to-rest motion task was considered for which the task duration (final time) was  $t_f = 0.4$  sec when applying the time-optimal control input. This yielded a travel distance of  $\gamma = 6.7$  cm. Figure ?? shows the experimental results. Note that applying the time-optimal con-

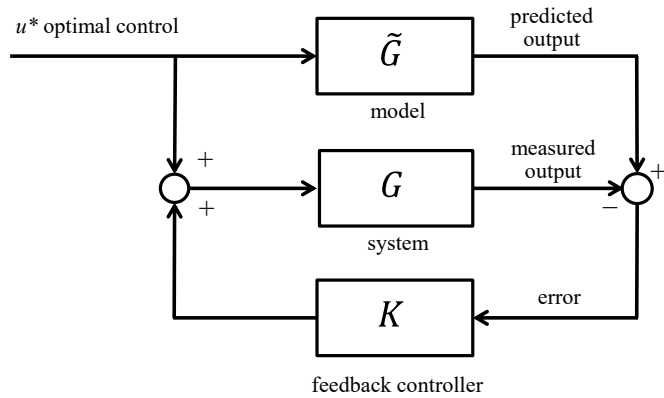
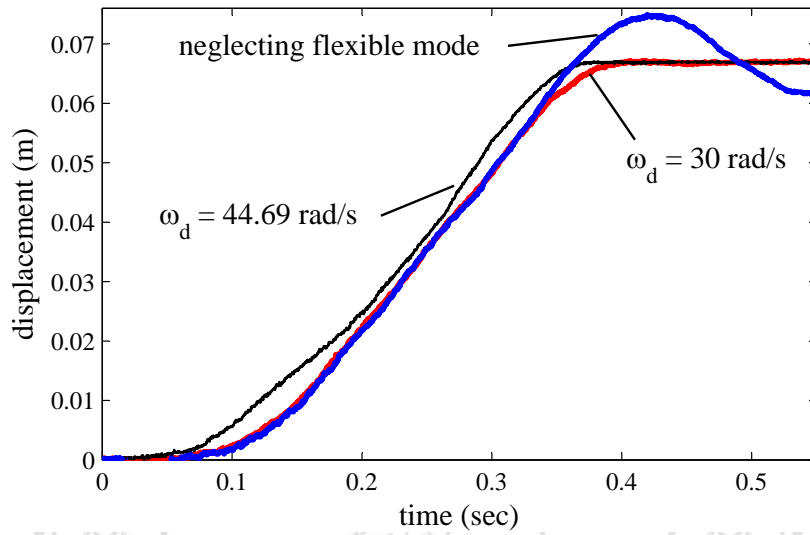


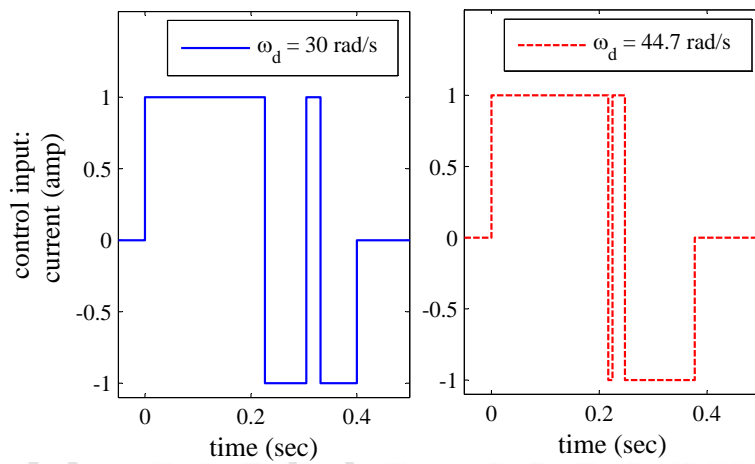
Figure 6.4: Block diagram of the controlled system with feedback loop

control input based on a rigid-body model gives a motion time of  $t_f = 0.375$  sec for the same travel-distance. However, residual vibration is significant.

The acquired time-optimal motion solution serves as the initial solution for the structural tuning algorithm. The numerical results indicated that a reduction in final time to  $t_f = 0.377$  sec could be achieved with  $\omega_d = 44.69$  rad/s, which is the local minimum point. The reduction in final time achieved in this case is about 5 percent of the initial value. The experimental data shown in Fig. ?? confirms that this solution can be implemented and is effective in achieving low residual vibration and a shorter motion duration compared with the unoptimized structure.



(a) Measured end displacement



(b) Time-optimal control inputs

Figure 6.5: Experimental results for rest-to-rest motions with un-optimized and optimized beam structures

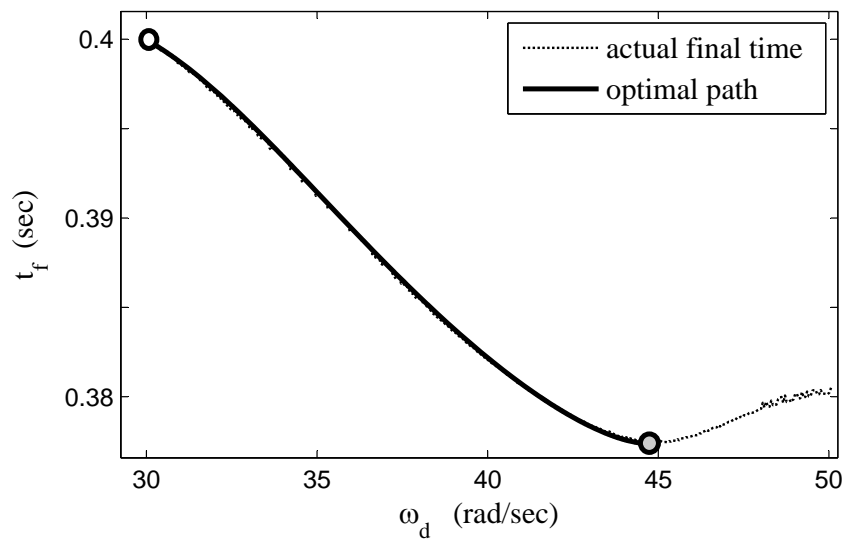


Figure 6.6: Convergence and cost function of the experiment

ลิขสิทธิ์มหาวิทยาลัยเชียงใหม่  
 Copyright© by Chiang Mai University  
 All rights reserved